EAI Endorsed Transactions
on Industrial Networks and Intelligent Systems
Research Article EAI.EU

Performance Analysis for RF Energy Harvesting Mobile Edge Computing Networks with SIMO/MISO-NOMA Schemes

Dac-Binh Ha[1,*], Van-Truong Truong[2], Yoonill Lee[3]

[1]Faculty of Electrical-Electronic Engineering, Duy Tan University, Da Nang, 550000, Vietnam and the Institute of Research and Development, Duy Tan University, Da Nang
[2]Faculty of Electrical-Electronic Engineering, Duy Tan University, Da Nang, 550000, Vietnam and the Institute of Research and Development, Duy Tan University, Da Nang
[3]Faculty of Electrical Engineering Technology at the College of Lake County, Grayslake, IL, USA

Abstract

In this paper, we study an RF energy harvesting mobile edge computing network based on a SIMO/MISO system and NOMA schemes over Nakagami-m fading. Specifically, a multi-antenna user harvests RF energy from a power station by using a selection combining/maximal ratio combining scheme and offload its tasks to two MEC servers through downlink NOMA by employing transmit antenna selection/maximal ratio transmission scheme. Accordingly, we investigate the performance of six schemes, namely SC-TAS1, SC-TAS1, MRC-TAS1, MRC-TAS2, SC-MRT, and MRC-MRT, for this considered system. To evaluate the performance, exact closed-form expressions of successful computation probability are derived. We further propose the optimal algorithm to find the best parameter sets to achieve the best performance. Moreover, the impacts of the network parameters on the system performance for these schemes are investigated. Finally, the simulation results are also provided to verify the accuracy of our analysis.

Received on 29 March 2021; accepted on 19 April 2021; published on 28 April 2021

Keywords: radio frequency energy harvesting, mobile edge computing, non-orthogonal multiple access, Nakagami-m fading, multi-antenna

doi:10.4108/eai.28-4-2021.169425

1. Introduction

Indeed, the next-generation wireless communication networks (NGWCN) (e.g., beyond 5G or 6G) will accommodate a massive number of user devices (e.g., Internet of Things (IoT)) and fulfill their capacity and computation demands [1]. However, it is beyond the possibility for existing wireless communication technologies with limited radio resources (e.g., spectrum and transmit power) and limited computation ability (i.e., computing and storing) to cope with such ever increasing capacity and computation demands.

Therefore, multiple candidate technologies (e.g., 3D MIMO, massive MIMO, mmWave, cognitive radio, cooperative communications, NOMA, intelligent reflecting surfaces, MEC, and so on) are needed be integrated into NGWCN to solve the rapidly growing problem of users. Among these technologies, the NOMA technique has been also recognized as an emerging technique for NGWCN because it can improve spectral efficiency and user fairness, and low transmission latency and higher cell-edge throughput [1–3]. This technique allows multiple users to share the same resource (e.g., a time/frequency domain) and separate the users in the power domain by exploiting successive interference cancellation (SIC) scheme at the receiver. Recently, many studies on the advancements needed in the transmitter and receiver sides for adopting NOMA schemes have been published [4–7].

Besides, some link-level and system-level performance evaluations have shown the potential of applying NOMA schemes in NGWCNs [8–10]. In addition, applications

*Corresponding author. Email: hadacbinh@duytan.edu.vn

of multiple antennas selection or combination schemes to NOMA systems have also been exploited to improve system performance [11–13]. The technique of transmit antenna selection (TAS) or maximal ratio transmission (MRT) can be deployed at the transmitter to assist the data transmission. The adaptive transmission mode switching between minimum mean square error beamforming and NOMA-based MRT for a system with one multi-antenna base station and two single-antenna users is investigated in [11]. In the work of [12], the system performance of a two-user cooperative multiple-input single-output (MISO) NOMA network with simultaneous wireless information and power transfer was investigated, where multiple antennas at source are exploited by utilizing TAS. The authors in [13] examined a TAS scheme and a user selection method to enhance the secrecy performance of the downlink MISO NOMA system.

Mobile edge computing (MEC) has been seen as a new evolution of cloud computing, in which the function of servers or access points moves towards the network edges to support the intensive computation needs of wireless devices in NGWCNs [14–18]. In this kind of computing approach, the edge servers serve as the computational access points to help accomplish the computation tasks of mobile computation-constrained devices through wireless links. There are two modes of computation offloading for mobile users: binary computation offloading and partial computation offloading. In binary computation offloading mode, the computation task that is highly integrated or relatively simple cannot be divided and has to be executed locally by itself or offloaded to the MEC servers. Meanwhile, in partial computation offloading mode, the computation task can be divided into two parts, one executed at the mobile device and the other offloaded to edge servers or access points. Some studies have investigated the combination of MEC with the NOMA technique to improve system performance in NGWCNs [19–22].

An uplink NOMA MEC system consisting of one multi-antenna base station (BS) and multiple single-antenna users is studied in [19]. In [20], the authors proposed a model that multiple users simultaneously offload their workload to one multi-antenna BS. The Lagrange method is used to solve the problem of optimizing the user's energy consumption. The offloading scheme in three different modes, namely the partial computation offloading, the complete local computation, and the complete offloading, was proposed in [21] for a NOMA MEC network, in which two users may partially offload their respective tasks to a single antenna MEC server through the uplink NOMA. The optimal solutions for an optimization problem to maximize the successful computation probability were obtained by jointly optimizing the parameters of this proposed scheme. The work of [22] studied NOMA MEC networks for both uplink and downlink transmissions in a general MEC communication scenario with multiple single-antenna users and multiple single-antenna access points. The studied results have shown that the use of NOMA can efficiently reduce the latency and energy consumption of MEC offloading compared to their conventional orthogonal multiple access (OMA) schemes.

Meantime, due to the energy-constrained wireless devices, the radio frequency energy harvesting (RF EH) technique is proposed and deployed in applications with quality-of-service requirements to prolong mobile users lifetime and maintain the coverage of wireless networks [23–25]. The prior research results have shown that the user computation performance can be improved by integrating RF EH and NOMA techniques into MEC networks [26–29]. Specifically, the IoT sensor nodes in [26] and the smart wearable devices in [27] can harvest RF energy and offload the heavy computation workload to the MEC server to satisfy the allowed delay under limited energy conditions. A similar model is proposed in [28], in which each user device can execute its task either locally at the mobile or by offloading to MEC using the energy harvesting from a single antenna base station. The joint computation offloading and resource allocation scheme is developed for the MEC system supporting multiple EH mobiles. A computation efficiency maximization framework was proposed for wireless-powered MEC networks based on uplink NOMA according to both partial and binary computation offloading modes [29]. The iterative algorithm and alternative optimization algorithm were proposed to solve the computation efficiency non-convex problem. The NOMA-MEC model is particularly suitable for applications with demanding time and energy requirements such as autonomous vehicles [30], Industrial Internet [31], Wearable Virtual Reality device [32].

Besides, receiver can employ selection combining (SC) or maximal ratio combining (MRC) technique for combining signals to improve the system performance [33, 34]. In work [34], the authors proposed a MEC network in which two multi-antenna computational access points support computation for a user under Nakagami- m fading. The operating protocol for the system is a combination of employ receiver antenna selection (RAS) or maximal ratio combining (MRC) at the receiver and implement selection combining (SC) or switch-and-stay combining (SSC). The paper concludes that the increased number of antennas helps improve system performance, i.e., reduce the latency and energy consumption effectively.

To the best of our knowledge, there is no prior work to study the integration of RF EH, multi-antenna technique, and downlink NOMA into MEC system. In

this work, we consider the scenario that a single multi-antenna user harvests the energy from the power station by using SC/MRC schemes and partially offloads its tasks to two MEC access points by applying TAS/MRT downlink NOMA schemes. We compared the system performance under protocols in term of successful computation probability (SCP). The main contributions of our paper are as follows.

- Six quadra-phase protocols for RF EH downlink NOMA mobile edge computing system based on SC/MRC and TAS/MRT schemes are proposed.
- Exact closed-form expressions of successful computation probability for these protocols of the considered system are derived.
- Two algorithms are proposed to find the optimal parameter set to achieve the best performance for this proposed system.
- The impact of the network parameters, e.g., transmit power, time switching ratio, power allocation ratio, and task bit allocation, on the system performance is examined by numerical results to verify the efficiency and effectiveness of deployment of RF EH, multi-antenna, and NOMA in MEC network.

The remainder of this paper is organized as follows. Section II presents the proposed system model. The performance analysis and optimization of this considered system are provided in Section III. The numerical results and discussion are shown in Section IV. Finally, we draw a conclusion for our work in Section V.

2. System and Channel Model

We define the notations used in the next part of this work in Table 1.

Fig. 1 depicts an RF EH NOMA MEC system in which an energy-constrained K-antenna user (**S**) harvests RF energy from a single antenna power station (**P**) to offload its task to two MEC servers located at single antenna access points (**AP**s). Specifically, **S** has tasks with L bits/task to be executed. Due to the constraint of latency requirement and its limited computation ability, it may not execute its tasks locally. Therefore, it offloads its tasks to MEC servers, which have more strong computation ability. However, due to the limited battery problem, **S** has to harvest RF energy by exploiting SC/MRC schemes and uses it to offload its tasks. After RF energy harvesting, it transmits its task data using all harvested energy based on TAS/MRT and downlink NOMA schemes. We assume that the task follows data-partition model and can be arbitrarily divided into different subtasks [35–37] to apply NOMA. For instance, $L_1 = \epsilon L$ ($0 \leq \epsilon \leq 1$) bits are offloaded to AP_1, and the remained $L_2 = (1-\epsilon)L$ bits are offloaded to AP_2. Finally, APs return the computing results to the user by the uplink NOMA scheme. The time flowchart of this considered RF EH NOMA MEC system is shown as Fig. 2.

TABLE 1. Notations

Notation	Meaning
m_0,m_1,m_2	Fading severity factor of Nakagami-m
g_0,g_1,g_2	Channel power gain of the wireless links of **P**-**S**, **S**-$\mathbf{AP}_1$, **S**-$\mathbf{AP}_2$
α	Time switching ratio
a	Power allocation coefficient
K	Number of antennas of **S**
P_0	Transmit power of power station **P**
γ_0	Average transmit SNR
η	Energy conversion efficiency
f_i	CPU-cycle frequency of $\mathbf{AP}_i$
ϵ	Task bit allocation coefficient
c_i	The number of required CPU cycles for each bit of $\mathbf{AP}_i$
B	Channel bandwidth
T	The threshold of latency
L	The length of task
Ps	Successful computation probability
δ	The algorithm accuracy factor

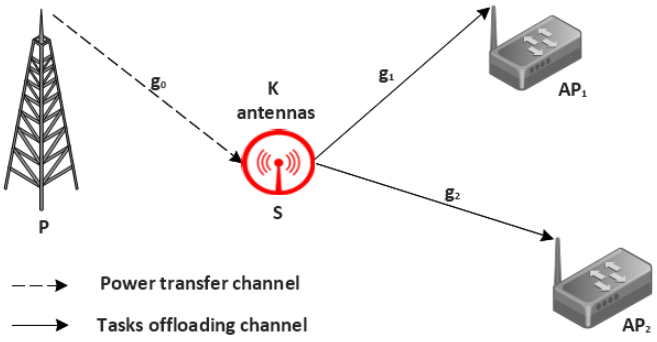

Figure 1. System Model for RF Energy Harvesting NOMA MEC Network

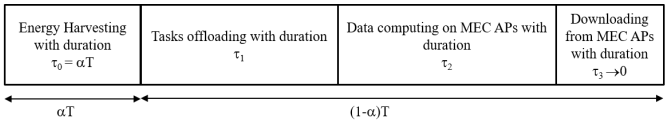

Figure 2. Time flowchart of the considered RF EH NOMA MEC system

The entire protocol can divide into four phases as **Algorithm 1**. Specifically,

• In the first phase (energy harvesting phase), **S** harvests energy from **P** during the time of $\tau_0 = \alpha T$, where α denotes the time switching ratio, i.e., $0 < \alpha < 1$, and T stands for transmission block time.

• In the second phase (offloading phase), **S** offloads its tasks to **AP**s in duration τ_1.

• In the third phase (computing phase), after successful transmission, the offloaded tasks are computed at the corresponding MEC **AP**s during duration τ_2.

• In the last phase (result downloading phase): After successful computation, the MEC **AP**s feedback the computed results to **S** within τ_3. Notice that due to the computed results is small data, we assume that τ_3 is very small compared to τ_0, τ_1 as well as τ_2 and thus is neglected [21, 29].

Assuming that all the channels have block Nakagami-m fading, i.e., the channel power gain is constant over each block but vary independently between between different block and follows Nakagami-m distribution with parameter m. We also assume that **P**, **S**, **AP**s operate in half-duplex mode and all harvested energy is used for offloading transmission. Let $\mathbf{h}_0 = [h_{01}, ..., h_{0K}]^T$, $\mathbf{h}_1 = [h_{11}, ..., h_{1K}]^T$ and $\mathbf{h}_2 = [h_{21}, ..., h_{2K}]^T$ denote the channel vectors of the wireless links **P** - **S**, **S** - $\mathbf{AP}_1$ and **S** - $\mathbf{AP}_2$, respectively.

Given the energy harvesting phase, the harvested energy of **S** during the duration of αT is given by

$$E = \eta P_0 g_0 \alpha T, \tag{1}$$

where $0 < \eta \leq 1$ stands for the energy conversion efficiency of the energy receiver [24], P_0 denotes the transmit power of power station, g_0 is the channel power gain of link **P** - **S**.

For the SC technique, an antenna at **S** is selected for RF EH to maximize the channel gain of the link **P** - **S**. Thus, the channel power gain g_0 is written as

$$g_0 = \max_{1 \leq k \leq K} (|h_{0k}|^2). \tag{2}$$

For the MRC technique, all of K antennas of **S** are used for RF EH to maximize the power harvesting. Therefore, the channel power gain g_0, in this case, is calculated as

$$g_0 = ||\mathbf{h}_0||^2. \tag{3}$$

Without loss of generality, we assume that the transmit power allocated to $\mathbf{AP}_1$ is greater than that allocated to $\mathbf{AP}_2$, thus a is selected to satisfy the condition: $0.5 < a \leq 1$ to apply the NOMA scheme. **S** broadcasts the signal to **AP**s by exploiting TAS/MRT schemes with transmit power P_T calculated as follows

$$P_T = \frac{E}{(1-\alpha)T} = \frac{\eta P_0 g_0 \alpha}{(1-\alpha)} = b P_0 g_0, \tag{4}$$

where $b \triangleq \frac{\eta\alpha}{(1-\alpha)}$.

During the offloading phase, **S** uses harvested energy to transmit a superimposed message signal

$$x = \sqrt{aP_T} s_1 + \sqrt{(1-a)P_T} s_2, \tag{5}$$

to **AP**s, where s_1 and s_2 are the messages for $\mathbf{AP}_1$ and $\mathbf{AP}_2$, respectively; a stands for the power allocation coefficient.

Thus, the received signals at $\mathbf{AP}_i$ corresponding to the k^{th} antenna of **S** is written as

$$y_{ik} = \left(\sqrt{aP_T} s_1 + \sqrt{(1-a)P_T} s_2\right) h_{ik} + n_{ik}, \tag{6}$$

where n_{ik} is the additive white Gaussian noise (AWGN) with mean 0 and variance σ^2 at $\mathbf{AP}_i$, $i \in \{1, 2\}$.

For applying the TAS scheme, an antenna at **S**, denoted as k^*, is selected for transmission to maximize the channel gain of the link **S** - $\mathbf{AP}_1$, namely TAS1 case:

$$k^* = \arg \max_{1 \leq k \leq K} (|h_{1k}|^2). \tag{7}$$

Thus, in this TAS1 case, the channel power gains for the selected transmit antenna (k^*) of links **S** - $\mathbf{AP}_1$ and **S** - $\mathbf{AP}_2$ are given by

$$(g_1, g_2) = (|h_{1k^*}|^2, |h_{2k^*}|^2). \tag{8}$$

Similarly, an antenna at **S**, denoted as k^{**}, can be selected to maximize the channel gain of the link **S** - $\mathbf{AP}_2$, namely TAS2 case, in which k^{**} is obtained by

$$k^{**} = \arg \max_{1 \leq k \leq K} (|h_{2k}|^2). \tag{9}$$

In this TAS2 case, the channel power gains corresponding to the selected transmit antenna of links **S** - $\mathbf{AP}_1$ and **S** - $\mathbf{AP}_2$ are written as

$$(g_1, g_2) = (|h_{1k^{**}}|^2, |h_{2k^{**}}|^2). \tag{10}$$

For applying the MRT scheme, all of K antennas of **S** are used for communication. Therefore, the channel power gains, in this case, are expressed as

$$g_i = ||\mathbf{h}_i||^2, i \in \{1, 2\}. \tag{11}$$

The instantaneous signal-to-interference-noise ratio (SINR) at $\mathbf{AP}_1$ to detect s_1 is given by

$$\gamma_{\mathbf{AP}_1}^{s_1} = \frac{ab\gamma_0 g_0 g_1}{(1-a)b\gamma_0 g_0 g_1 + 1}, \tag{12}$$

where $\gamma_0 \triangleq \frac{P_0}{\sigma^2}$ is the average transmit signal-to-noise ratio (SNR).

By applying successive interference cancellation (SIC) technique, $\mathbf{AP}_2$ detects message s_1 and subtracts this component from the received signal to obtain its message s_2. Therefore, the instantaneous SINR at $\mathbf{AP}_2$ to detect

s_1 is obtained by

$$\gamma_{\mathbf{AP}_2}^{s_1} = \frac{ab\gamma_0 g_0 g_2}{(1-a)b\gamma_0 g_0 g_2 + 1}, \quad (13)$$

and the instantaneous SNR at $\mathbf{AP}_2$ to detect s_2 is written as

$$\gamma_{\mathbf{AP}_2}^{s_2} = (1-a)b\gamma_0 g_0 g_2. \quad (14)$$

The instantaneous channel capacity of link **S** - $\mathbf{AP}_1$ and link **S** - $\mathbf{AP}_2$ are respectively obtained by

$$C_1 = (1-\alpha)B\log_2\left(1+\gamma_{\mathbf{AP}_1}^{s_1}\right), \quad (15)$$
$$C_2 = (1-\alpha)B\log_2\left(1+\gamma_{\mathbf{AP}_2}^{s_2}\right), \quad (16)$$

where B is the channel bandwidth.

The transmission latencies of offloading to $\mathbf{AP}_1$ and $\mathbf{AP}_2$ are respectively expressed as

$$t_1 = \frac{\epsilon L}{(1-\alpha)B\log_2\left(1+\gamma_{\mathbf{AP}_1}^{s_1}\right)}, \quad (17)$$
$$t_2 = \frac{(1-\epsilon)L}{(1-\alpha)B\log_2\left(1+\gamma_{\mathbf{AP}_2}^{s_2}\right)}, \quad (18)$$

where ϵ denotes the task bit allocation coefficient.

The execution time τ of this system is calculated as follows

$$\tau = \max\left\{t_1 + \frac{c_1\epsilon L}{f_1}, t_2 + \frac{c_2(1-\epsilon)L}{f_2}\right\}, \quad (19)$$

where c_i denotes the number of required CPU cycles for each bit of $\mathbf{AP}_i$, and f_i stands for the CPU-cycle frequency at the $\mathbf{AP}_i$, $i \in \{1,2\}$.

The SC-TAS1, SC-TAS2, MRC-TAS1, MRC-TAS2, SC-MRT, MRC-MRT schemes for this considered system are summarized as **Algorithm 1**.

Algorithm 1 Proposed quadra-phase schemes for RF EH NOMA MEC system

1: **procedure** RF EH NOMA MEC Protocol
Setup:
2: Selection: SC-TAS1, SC-TAS2, MRC-TAS1, MRC-TAS2, SC-MRT, MRC-MRT
Loop:
3: **Phase-1**: **S** harvests energy from **P** by exploiting SC/MRC scheme.
4: **Phase-2**: **S** broadcasts its tasks to **AP**s by applying TAS1/TAS2/MRT and NOMA schemes. $\mathbf{AP}_2$ uses SIC technique to detect s_2.
5: **Phase-3**: **S** waits for **AP**s execute the received tasks.
6: **Phase-4**: **S** downloads the computed results from **AP**s.
7: **end procedure**

Notice that the wireless links of **P** - **S**, **S** - $\mathbf{AP}_1$ and **S** - $\mathbf{AP}_2$ undergo the Nakagami-m fading which is a generalized fading model for practical communication scenarios. Therefore, the cumulative distribution function (CDF) and probability density function (PDF) of channel power gains, i.e., $|h_{ik}|^2$, ($i \in \{0,1,2\}$ and $1 \le k \le K$) are respectively given by

$$F_{|h_{ik}|^2}(x) = 1 - e^{-\frac{m_i}{\lambda_i}x}\sum_{l=0}^{m_i-1}\frac{1}{l!}\left(\frac{m_i}{\lambda_i}x\right)^l, \quad (20)$$

$$f_{|h_{ik}|^2}(x) = \frac{1}{(m_i-1)!}\left(\frac{m_i}{\lambda_i}\right)^{m_i} x^{m_i-1}e^{-\frac{m_i}{\lambda_i}x}, \quad (21)$$

where $\lambda_i = \mathbf{E}(|h_{ik}|^2)$, $m_i \ge 1/2$ is the fading severity factor, in which $m_i = 1$ corresponds to Rayleigh fading and $m_i = (V+1)^2/(2V+1)$ approximates Rician fading with parameter V, $\mathbf{E}(.)$ stands for expectation operator.

For SC scheme, the CDF and PDF of g_0 can be respectively written as

$$F_{g_0}(x) = \left(1 - \sum_{l=0}^{m_0-1}\frac{m_0^l}{l!\lambda_0^l}x^l e^{-\frac{m_0}{\lambda_0}x}\right)^K = \sum_{k_0=0}^{K}\sum_{\sigma_0=k_0}\Phi_0 x^{\varphi_0}e^{-\frac{k_0 m_0}{\lambda_0}x}, \quad (22)$$

$$f_{g_0}(x) = \sum_{k_0=1}^{K}\sum_{\sigma_0=k_0}\Phi_0\left(\varphi_0 - \frac{k_0 m_0}{\lambda_0}x\right)x^{\varphi_0-1}e^{-\frac{k_0 m_0}{\lambda_0}x}, \quad (23)$$

where $\Phi_0 = \binom{K}{k_0}\binom{k_0}{\delta_0,\ldots,\delta_{m_0-1}}(-1)^{k_0}\prod_{l=0}^{m_0-1}\left(\frac{m_0^l}{l!\lambda_0^l}\right)^{\delta_l}$, $\sigma_0 = \sum_{l=0}^{m_0-1}\delta_l$, and $\varphi_0 = \sum_{l=0}^{m_0-1}l\delta_l$ [13].

Similarly, for TAS1 case, the CDF and PDF of g_1 can be respectively written as

$$F_{g_1}(x) = \left(1 - \sum_{l=0}^{m_1-1}\frac{m_1^l}{l!\lambda_1^l}x^l e^{-\frac{m_1}{\lambda_1}x}\right)^K = \sum_{k_1=0}^{K}\sum_{\sigma_1=k_1}\Phi_1 x^{\varphi_1}e^{-\frac{k_1 m_1}{\lambda_1}x}, \quad (24)$$

$$f_{g_1}(x) = \sum_{k_1=1}^{K}\sum_{\sigma_1=k_1}\Phi_1\left(\varphi_1 - \frac{k_1 m_1}{\lambda_1}x\right)x^{\varphi_1-1}e^{-\frac{k_1 m_1}{\lambda_1}x}, \quad (25)$$

where $\Phi_1 = \binom{K}{k_1}\binom{k_1}{\delta_0,\ldots,\delta_{m_1-1}}(-1)^{k_1}\prod_{l=0}^{m_1-1}\left(\frac{m_1^l}{l!\lambda_1^l}\right)^{\delta_l}$, $\sigma_1 = \sum_{l=0}^{m_1-1}\delta_l$, and $\varphi_1 = \sum_{l=0}^{m_1-1}l\delta_l$. It follows that the CDF and PDF of g_2 can be respectively given by

$$F_{g_2}(x) = 1 - e^{-\frac{m_2}{\lambda_2}x}\sum_{l=0}^{m_2-1}\frac{1}{l!}\left(\frac{m_2}{\lambda_2}x\right)^l, \quad (26)$$

$$f_{g_2}(x) = \frac{1}{(m_2-1)!}\left(\frac{m_2}{\lambda_2}\right)^{m_2} x^{m_2-1}e^{-\frac{m_2}{\lambda_2}x}. \quad (27)$$

Similarly, for TAS2 case, the CDF and PDF of g_1 can be respectively expressed as

$$F_{g_1}(x) = 1 - e^{-\frac{m_1}{\lambda_1}x}\sum_{l=0}^{m_1-1}\frac{1}{l!}\left(\frac{m_1}{\lambda_1}x\right)^l, \quad (28)$$

$$f_{g_1}(x) = \frac{1}{(m_1-1)!}\left(\frac{m_1}{\lambda_1}\right)^{m_1} x^{m_1-1}e^{-\frac{m_1}{\lambda_1}x}. \quad (29)$$

It follows that the CDF and PDF of g_2 in this case can be respectively written as

$$F_{g_2}(x) = \sum_{k_2=0}^{K}\sum_{\sigma_2=k_1}\Phi_2 x^{\varphi_2}e^{-\frac{k_2m_2}{\lambda_2}x}, \quad (30)$$

$$f_{g_2}(x) = \sum_{k_2=1}^{K}\sum_{\sigma_2=k_2}\Phi_2\left(\varphi_2 - \frac{k_2m_2}{\lambda_2}x\right)x^{\varphi_2-1}e^{-\frac{k_2m_2}{\lambda_2}x}, \quad (31)$$

where $\Phi_2 = \binom{K}{k_2}\binom{k_2}{\delta_0,\ldots,\delta_{m_2-1}}(-1)^{k_2}\prod_{l=0}^{m_2-1}\left(\frac{m_2^l}{l!\lambda_2^l}\right)^{\delta_l}$, $\sigma_2 = \sum_{l=0}^{m_2-1}\delta_l$, and $\varphi_2 = \sum_{l=0}^{m_2-1} l\delta_l$.

For MRT/MRC scheme, the CDF and PDF of g_i can be respectively expressed as

$$F_{g_i}^{MRT/MRC}(x) = 1 - \sum_{l=0}^{m_iK-1}\frac{m_i^l}{l!\lambda_i^l}x^l e^{-\frac{m_i}{\lambda_i}x}, \quad (32)$$

$$f_{g_i}^{MRT/MRC}(x) = \frac{1}{(m_iK-1)!}\left(\frac{m_i}{\lambda_i}\right)^{m_iK} x^{m_iK-1}e^{-\frac{m_i}{\lambda_i}x}. \quad (33)$$

where $i \in \{0,1,2\}$.

3. Performance Analysis and Optimization

In this section, we present the performance analysis of this proposed system in terms of the successful computation probability (Ps) and the optimization of the parameter set to achieve the optimal performance.

3.1. Performance analysis

In order to characterize the performance of a MEC system, Ps is defined as the probability that all tasks are successfully executed within a given time $T_{th} > 0$ [21]. Therefore, Ps of this proposed system is written as

$$Ps = Pr(\tau < T_{th}) = Pr\left(\tau < (1-\alpha)T\right), \quad (34)$$

where τ is calculated as (19).

In order to evaluate the performance of six schemes, i.e., SC-TAS1, SC-TAS2, MRC-TAS1, MRC-TAS2, SC-MRT, MRC-MRT, for this considered RF EH NOMA MEC system, we obtain the following theorem.

Theorem 1. Under Nakagami-m fading, the exact closed form expressions of the successful computation probability Ps for this considered RF EH MEC system based on SC-TAS1, SC-TAS2, MRC-TAS1, MRC-TAS2, SC-MRT, MRC-MRT downlink NOMA schemes, respectively, is given by formula SCP.

where $\rho = 1 - \frac{1}{2^{\frac{\epsilon L}{\Omega_1 B}}}$, $\Psi_1 = \frac{2^{\frac{\epsilon L}{(1-\alpha)B\Omega_1}}-1}{\gamma_s\left[a-(1-a)\left(2^{\frac{\epsilon L}{(1-\alpha)B\Omega_1}}-1\right)\right]}$, $\Psi_2 = \frac{2^{\frac{(1-\epsilon)L}{(1-\alpha)B\Omega_2}}-1}{(1-a)\gamma_s}$, $\Omega_1 = (1-\alpha)T - \frac{c_1\epsilon L}{f_1}$, $\Omega_2 = (1-\alpha)T - \frac{c_2(1-\epsilon)L}{f_2}$,
$v_1 = \varphi_0 - \varphi_1 - l$, $\beta_1 = \frac{k_1m_1\Psi_1}{\lambda_1} + \frac{m_2\Psi_2}{\lambda_2}$, $\mu_1 = \frac{k_0m_0}{\lambda_0}$,
$v_2 = \varphi_0 - \varphi_2 - l$, $\beta_2 = \frac{m_1\Psi_1}{\lambda_1} + \frac{k_2m_2\Psi_2}{\lambda_2}$, $\mu_2 = \frac{k_0m_0}{\lambda_0}$,
$v_3 = m_0K - \varphi_1 - l$, $\beta_3 = \frac{k_1m_1\Psi_1}{\lambda_1} + \frac{m_2\Psi_2}{\lambda_2}$, $\mu_3 = \frac{m_0}{\lambda_0}$,
$v_4 = m_0K - \varphi_2 - l$, $\beta_4 = \frac{m_1\Psi_1}{\lambda_1} + \frac{k_2m_2\Psi_2}{\lambda_2}$, $\mu_4 = \frac{m_0}{\lambda_0}$,
$v_5 = \varphi_0 - l_1 - l_2$, $\beta_5 = \frac{m_1\Psi_1}{\lambda_1} + \frac{m_2\Psi_2}{\lambda_2}$, $\mu_5 = \frac{k_0m_0}{\lambda_0}$,
$v_6 = m_0K - l_1 - l_2$, $\beta_6 = \frac{m_1\Psi_1}{\lambda_1} + \frac{m_2\Psi_2}{\lambda_2}$, $\mu_6 = \frac{m_0}{\lambda_0}$,
and $\mathcal{K}_v(.)$ is the modified Bessel function of the second kind and v^{th} order.

Proof. See in Appendix A. □

Remark 1. The condition $a > \rho = 1 - \frac{1}{2^{\frac{c_1\epsilon L}{\Omega_1 B}}}$ in Equation SCP is constraint of three key parameters: data offloading ratio (ϵ), time switching ratio (α), and power allocation ratio (a). This constraint can be rewritten as follows:

$$(1-a)2^{\frac{\epsilon L}{\left[(1-\alpha)T - \frac{c_1\epsilon L}{f_1}\right]B}} < 1. \quad (35)$$

3.2. Optimization: Problem formulation and solution

According to the above analysis, we formulate the optimization problem to maximize Ps as follows:

$$(\text{SCPMP}): \max_{\epsilon,\alpha,a}(Ps) \quad (36a)$$

$$\text{subject to} \quad 0 \le \epsilon \le 1 \quad (36b)$$

$$0 < \alpha \le 1 \quad (36c)$$

$$0.5 < a \le 1 \quad (36d)$$

Note: SCPMP stands for successful computation probability maximization problem. Constraint (36b) describes the data offloading ratio for **AP**s. Constraint (36c) describes the time switching ratio for energy harvesting. Constraint (36d) means that the power allocation ratio is chosen to apply NOMA and maximize Ps. To solve (36), we propose two optimal algorithms: **Algorithm 2 - SCPMS** and **Algorithm 3 - SCPMG**, which is used to find the optimal set $(Ps_{\max}, \epsilon^*, \alpha^*, a^*)$ in the entire solution space.

The **Algorithm 2 - SCPMS** is based on search method and is divided into two simple steps. We use

$$Ps = \begin{cases} 0, & \text{if } a < \rho, \text{All of schemes} \\ \sum_{k_0=1}^{K}\sum_{k_1=1}^{K}\sum_{l=0}^{m_2-1}\sum_{\sigma_0=k_0}\sum_{\sigma_1=k_1}\frac{2}{l!}\Phi_0\Phi_1\Psi_1^{\varphi_1}\Psi_2^{\varphi_2}\left(\frac{m_2}{\lambda_2}\right)^l\left(\frac{\beta_1}{\mu_1}\right)^{\frac{v_1}{2}} & \\ \times\left[\varphi_0\mathcal{K}_{v_1}\left(2\sqrt{\beta_1\mu_1}\right)-\sqrt{\beta_1\mu_1}\mathcal{K}_{v_1+1}\left(2\sqrt{\beta_1\mu_1}\right)\right], & \text{if } a > \rho, \text{SC-TAS1, (a)} \\ \sum_{k_0=1}^{K}\sum_{l=0}^{m_1-1}\sum_{k_2=1}^{K}\sum_{\sigma_0=k_0}\sum_{\sigma_2=k_2}\frac{2}{l!}\Phi_0\Phi_2\Psi_1^{\varphi_1}\Psi_2^{\varphi_2}\left(\frac{m_1}{\lambda_1}\right)^l\left(\frac{\beta_2}{\mu_2}\right)^{\frac{v_2}{2}} & \\ \times\left[\varphi_0\mathcal{K}_{v_2}\left(2\sqrt{\beta_2\mu_2}\right)-\sqrt{\beta_2\mu_2}\mathcal{K}_{v_2+1}\left(2\sqrt{\beta_2\mu_2}\right)\right], & \text{if } a > \rho, \text{SC-TAS2, (b)} \\ \frac{2}{(m_0K-1)!}\left(\frac{m_0}{\lambda_0}\right)^{m_0K}\sum_{k_1=1}^{K}\sum_{\sigma_1=k_1}\sum_{l=0}^{m_2-1}\frac{\Phi_1\Psi_1^{\varphi_1}}{l!}\left(\frac{m_2\Psi_2}{\lambda_2}\right)^l\left(\frac{\beta_3}{\mu_3}\right)^{\frac{v_3}{2}}\mathcal{K}_{v_3}\left(2\sqrt{\beta_3\mu_3}\right), & \text{if } a > \rho, \text{MRC-TAS1, (c)} \\ \frac{2}{(m_0K-1)!}\left(\frac{m_0}{\lambda_0}\right)^{m_0K}\sum_{l=0}^{m_1-1}\sum_{k_2=1}^{K}\sum_{\sigma_2=k_2}\frac{\Phi_2\Psi_2^{\varphi_2}}{l!}\left(\frac{m_1\Psi_1}{\lambda_1}\right)^l\left(\frac{\beta_4}{\mu_4}\right)^{\frac{v_4}{2}}\mathcal{K}_{v_4}\left(2\sqrt{\beta_4\mu_4}\right), & \text{if } a > \rho, \text{MRC-TAS2, (d)} \\ \sum_{k_0=1}^{K}\sum_{\sigma_0=k_0}\sum_{l_1=0}^{m_1K-1}\sum_{l_2=0}^{m_2K-1}\frac{2\Phi_0}{l_1!l_2!}\left(\frac{m_1\Psi_1}{\lambda_1}\right)^{l_1}\left(\frac{m_2\Psi_2}{\lambda_2}\right)^{l_2}\left(\frac{\beta_5}{\mu_5}\right)^{\frac{v_5}{2}} & \\ \times\left[\varphi_0\mathcal{K}_{v_5}\left(2\sqrt{\beta_5\mu_5}\right)-\sqrt{\beta_5\mu_5}\mathcal{K}_{v_5+1}\left(2\sqrt{\beta_5\mu_5}\right)\right], & \text{if } a > \rho, \text{SC-MRT, (e)} \\ \frac{1}{(m_0K-1)!}\left(\frac{m_0}{\lambda_0}\right)^{m_0K}\sum_{l_1=0}^{m_1K-1}\sum_{l_2=0}^{m_2K-1}\frac{2}{l_1!l_2!}\left(\frac{m_1\Psi_1}{\lambda_1}\right)^{l_1}\left(\frac{m_2\Psi_2}{\lambda_2}\right)^{l_2}\left(\frac{\beta_6}{\mu_6}\right)^{\frac{v_6}{2}}\mathcal{K}_{v_6}\left(2\sqrt{\beta_6\mu_6}\right), & \text{if } a > \rho, \text{MRC-MRT, (f)} \end{cases} \quad \text{(SCP)}$$

three loops to cover the entire solution space (ϵ, α, a). First, depending on which one of the six schemes the system operates, Ps is calculated with the right formula. Next, for each set of parameters (ϵ, α, a), we evaluate Ps and update Ps_{max}. The algorithm terminates when (ϵ, α, a) approach their upper limit, i.e., $\epsilon = 1, \alpha = 1$ and $a = 1$. We define δ is an accuracy factor, that is, the step where each parameter in (ϵ, α, a) is updated in each loop. The smaller δ, the higher the accuracy. Thus, the total number of comparison operations that the **SCPMS** algorithm needs to perform is given by:

$$\frac{\epsilon_{max} - \epsilon_{min}}{\delta} \cdot \frac{\alpha_{max} - \alpha_{min}}{\delta} \cdot \frac{a_{max} - a_{min}}{\delta} \tag{37}$$

As such, the complexity complexity of algorithm **SCPMS** is $O(\frac{1}{\delta}^3)$.

We propose the second algorithm for the SCPMP based on the Golden section search algorithm, i.e., the **SCPMG**. **Algorithm 3 – SCPMG** consists of four main steps:

- Step 1: Similar to **SCPMS** algorithm, **SCPMG** chooses the Ps formula according to the scheme that the system is operating.
- Step 2 (Initialization): Determine lower bound $x_l \triangleq (\epsilon_l, \alpha_l, a_l)$ and upper bound $x_u \triangleq (\epsilon_u, \alpha_u, a_u)$. We define δ is an accuracy factor. Normalize the variable a by using the equation

$$\hat{a} = \frac{a - a_l}{a_u - a_l} \tag{38}$$

  Thus, the interval of each parameter $(\epsilon, \alpha, \hat{a})$ is [0,1]. Determine two intermediate points $x_1 \triangleq (\epsilon_1, \alpha_1, a_1)$ and $x_2 \triangleq (\epsilon_2, \alpha_2, a_2)$ such that:

$$\begin{aligned} x_1 &= x_l + (x_u - x_l)/G, \\ x_2 &= x_u - (x_u - x_l)/G \end{aligned} \tag{39}$$

  where $G = \frac{\sqrt{5}+1}{2}$ is the golden ratio.
- Step 3 (Evaluation): Next, we evaluate Ps at x_1 and x_2. In case $Ps(x_1) > Ps(x_2)$, we update $x_l \leftarrow x_2, x_2 \leftarrow x_1$, and $x_1 \leftarrow x_l + (x_u - x_l)/G$. In the opposite case, we update $x_u \leftarrow x_1, x_1 \leftarrow x_2$, and $x_2 \leftarrow x_u - (x_u - x_l)/G$.
- Step 4: We run step continuously in the loop until $x_u - x_l < \delta$. Then, the algorithm terminates and the Ps_{max} occurs at $\frac{x_u + x_l}{2}$.

So, **SCPMG** use three loops that cut the interval in $\frac{1}{G}$ each time they run; hence, its time complexity is $O(\log^3(\frac{1}{\delta}))$.

4. Numerical Results and Discussion

In this section, we provide numerical results in terms of successful computation probability Ps for SC-TAS1, SC-TAS2, MRC-TAS1, MRC-TAS2, SC-MRT, MRC-MRT schemes to reveal the impacts of key system parameters (data offloading ratio, time switching ratio, and power allocation coefficient) to the system performance. Furthermore, the simulation results are also provided to verify analytical results. The parameters used in this work are provided in TABLE 2.

Algorithm 2 Successful computation probability maximization searching (SCPMS) algorithm

Input: $\gamma_0, L, c_1, c_2, f_1, f_2, T$
Output: $Optimalset\,(Ps_{\max}, \epsilon^*, \alpha^*, a^*)$
Initialize: $Optimalset(0,0,0,0)$
Parameters: $(\epsilon, \alpha, a) \leftarrow (0.01, 0.01, \max\{0.5, \rho\} + 0.01)$
Step: $\delta \leftarrow 0.01$
while $\epsilon \leq 1$ **do**
  while $\alpha \leq 1$ **do**
    while $a \leq 1$ **do**
      switch (Scheme)
      case SC-TAS1: Calculate Ps using SCP (a).
      case SC-TAS2: Calculate Ps using SCP (b).
      case MRC-TAS1: Calculate Ps using SCP (c).
      case MRC-TAS2: Calculate Ps using SCP (d).
      case SC-MRT: Calculate Ps using SCP (e).
      case MRC-MRT: Calculate Ps using SCP (f).
      endswitch
      if $(Ps > Ps_{\max})$ **then**
        Update $(Ps_{\max}, \epsilon^*, \alpha^*, a^*) \leftarrow (Ps_{\max}, \epsilon, \alpha, a)$
      end if
      Update $\epsilon \leftarrow \epsilon + \delta$
    end while
    Update $\alpha \leftarrow \alpha + \delta$
  end while
  Update $a \leftarrow a + \delta$
end while
Return $Optimalset\,(Ps_{\max}, \epsilon^*, \alpha^*, a^*)$

4.1. Impacts of average transmit SNR and the number of antennas

Figs. 3-8 depict the impacts of average transmit SNR γ_0 and the number of antennas K on Ps with $\epsilon = 0.6$, $\alpha = 0.3$, and $a = 0.8$. Obviously, from these figures we can observe that γ_0 or/and K increase leading Ps increases. It means that the computing performance of this considered system can be improved by increasing the average transmit SNR or/and the number of antennas. However, when γ_0 gets too large, Ps will tend to be saturated. So in the proposed model, it is not necessary to increase the transmit power of the user too large.

As expected, in above figures, we observe that the Ps of the NOMA scheme significantly outperforms that of the OMA scheme.

Algorithm 3 Successful computation probability maximization Golden searching (SCPMG) algorithm

Input: $\gamma_0, L, c_1, c_2, f_1, f_2, T$
Output: $Optimalset\,(Ps_{\max}, \epsilon^*, \alpha^*, a^*)$
Initialize: $Optimalset(0,0,0,0)$
Parameters: $x_l \triangleq (\epsilon_l, \alpha_l, a_l)$, $x_u \triangleq (\epsilon_u, \alpha_u, a_u)$
Step: $\delta \leftarrow 0.01$
Normalize a using (38)
Determine $x_1 \triangleq (\epsilon_1, \alpha_1, a_1)$ and $x_2 \triangleq (\epsilon_2, \alpha_2, a_2)$ using (39)
while $\epsilon_u - \epsilon_l > \delta$ **do**
  while $\alpha_u - \alpha_l > \delta$ **do**
    while $a_u - a_l > \delta$ **do**
      switch (Scheme)
      case SC-TAS1: Calculate Ps using SCP (a).
      case SC-TAS2: Calculate Ps using SCP (b).
      case MRC-TAS1: Calculate Ps using SCP (c).
      case MRC-TAS2: Calculate Ps using SCP (d).
      case SC-MRT: Calculate Ps using SCP (e).
      case MRC-MRT: Calculate Ps using SCP (f).
      endswitch
      if $(Ps(x_1) > Ps_(x_2))$ **then**
        Update $(Ps_{\max}, x_l, x_2, x_1) \leftarrow (Ps_{x_1}, x_2, x_1, x_l + (x_u - x_l)/G)$
      else
        Update $(Ps_{\max}, x_u, x_1, x_2) \leftarrow (Ps_{x_2}, x_1, x_2, x_u - (x_u - x_l)/G)$
      end if
    end while
  end while
end while
Return $Optimalset\,(Ps_{\max}, \epsilon^*, \alpha^*, a^*)$ at $\frac{x_u + x_l}{2}$

4.2. Impacts of the data offloading ratio

In Fig. 9, we examine Ps as a function of the data offloading ratio ϵ with $\gamma_0 = 10dB$, $K = 2$, $\alpha = 0.3$, and $a = 0.8$ for different schemes. From this figure, we can see that when ϵ increases from 0 to ϵ^*, Ps upgrades. However, if ϵ continuously increases from ϵ^* to 1, Ps degrades. This can be easily explained that applying NOMA $\mathbf{AP}_1$ is allocated more transmit power than $\mathbf{AP}_2$, therefore when ϵ increases, Ps upgrades. However, when ϵ continuously increases the load allocated for $\mathbf{AP}_1$ increases. This leads the offloading and computing time of $\mathbf{AP}_1$ longer and makes Ps degrades, meanwhile the $\mathbf{AP}_2$'s time is wasted.

TABLE 1. Simulation Parameters

Parameters	Notation	Typical Values
Environment		Nakagami-m
Fading severity factor of Nakagami-m	m_0,m_1,m_2	3, 2, 1
Number of antennas of **AP**s		1
Average transmit SNR	γ_0	0-30dB
Energy conversion efficiency	η	0.75
CPU-cycle frequency of $\mathbf{AP}_1$	f_1	5 GHz
CPU-cycle frequency of $\mathbf{AP}_2$	f_2	10 GHz
The number of CPU cycles for each bit	c_1, c_2	10
Channel bandwidth	B	100 MHz
The threshold of latency	T	0.5s
The length of task	L	80 Mbits

4.3. Impacts of the time switching ratio

The impacts of the time switching ratio α on Ps are depicted as Fig. 10 with $\gamma_0 = 10dB$, $K = 2$, $\epsilon = 0.6$, and $a = 0.8$ for different schemes. From this figure, we can observe that when α increases from 0 to α^*, Ps upgrades, when α continuously increases from α^* to 0.5, Ps degrades. When $\alpha \geq 0.5$, Ps is approximately 0 due to the condition (35). It can be explained that when α increases from 0 to α^*, the more harvested energy the better SNR and the better Ps. However, if α continuously increases the remained time for transmission and computation is less, this makes Ps degrades.

4.4. Impacts of the power allocation coefficient

In Fig. 11, we investigate Ps as a function of the power allocation coefficient a with $\gamma_0 = 10dB$, $K = 2$, $\epsilon = 0.6$, and $\alpha = 0.3$ for different schemes. From this figure, we can see that when a increases from $\max\{0.5, \rho\}$ to a^*, Ps upgrades and when a continuously increases from a^* to 1, Ps degrades. This can be easily explained that due to the offloading data for $\mathbf{AP}_1$ is larger the $\mathbf{AP}_2$, thus when a increasing leads $\mathbf{AP}_1$ allocated more transmit power than $\mathbf{AP}_2$, Ps upgrades. However, when a continuously increases the power allocated for $\mathbf{AP}_2$ decreases and makes Ps degrades.

Remark 2. From Figs. 3-11, we can see that the MRC-MRT scheme is the best one, meantime the SC-TAS1 scheme is worst one. This is reasonable because the MRC-MRT scheme employs all antennas to harvest RF energy and offload tasks to **AP**s, meanwhile in SC-TAS1 scheme only the best antenna is selected to harvest RF energy and offload task to **AP**s, but it is simplest one.

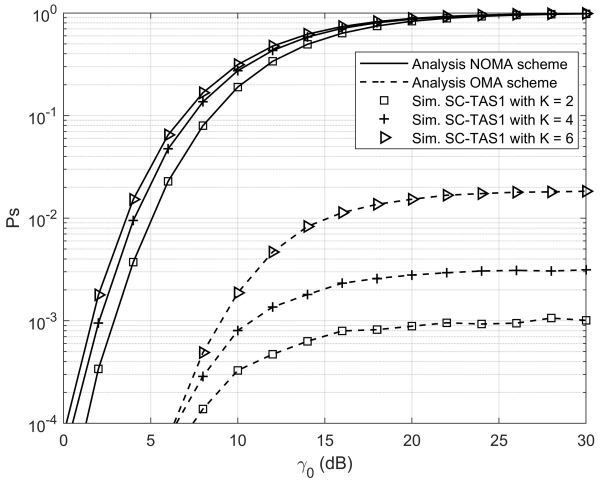

Figure 3. Impacts of the number of antennas K on Ps of SC-TAS1 scheme

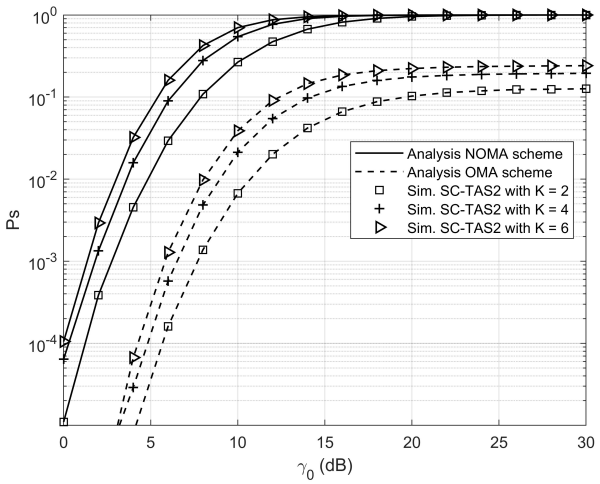

Figure 4. Impacts of the number of antennas K on Ps of SC-TAS2 scheme

Remark 3. From Figs. 3-11, we can observe that the analysis and simulation results are matching very well. It means that the correctness of our analysis has been verified.

4.5. Impacts of the length of task and the bandwidth

Figure 12 presents the Ps by the length of the task under different bandwidth. We fixed the power allocation to 0.8. We observe that Ps decreases when L increases. It can be explained as the time that spent on the offloading phase increases when L increases (follow a formula (17),

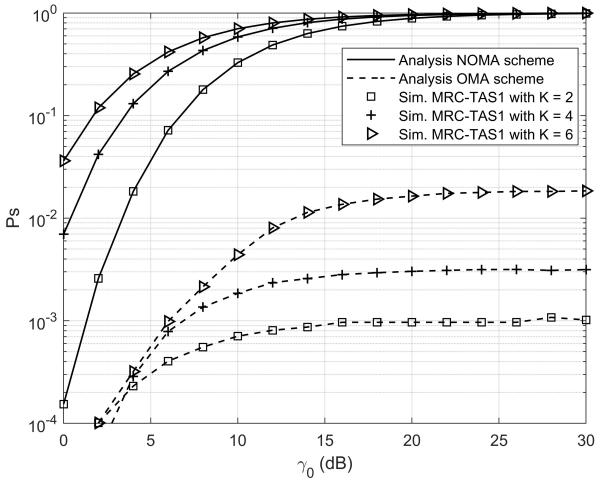

Figure 5. Impacts of the number of antennas K on Ps of MRC-TAS1 scheme

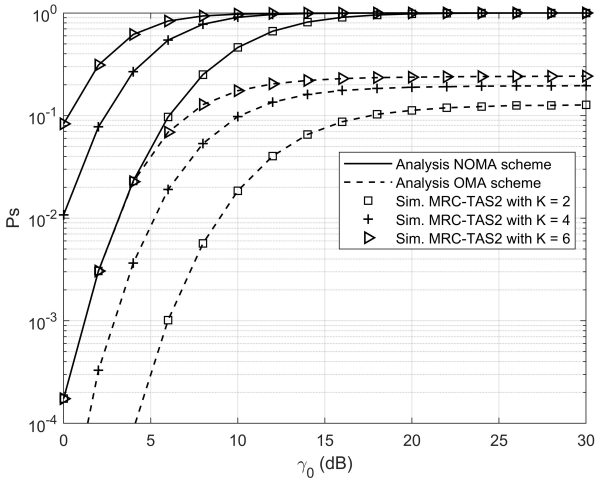

Figure 6. Impacts of the number of antennas K on Ps of MRC-TAS2 scheme

(18)), which reduces the time remaining for the data computing phase. Thus, both user and **APs** will likely not have enough time to handle all of their tasks, so the Ps decreases.

Figure 12 shows the apparent effect of bandwidth on system performance. The case where the bandwidth is sufficiently large (B = 100 MHz) offers much better performance than the lower bandwidth case (B = 50 MHz). In case the length of task is short, the effect of bandwidth is not significant, but the longer the task, the impact of bandwidth is very pronounced.

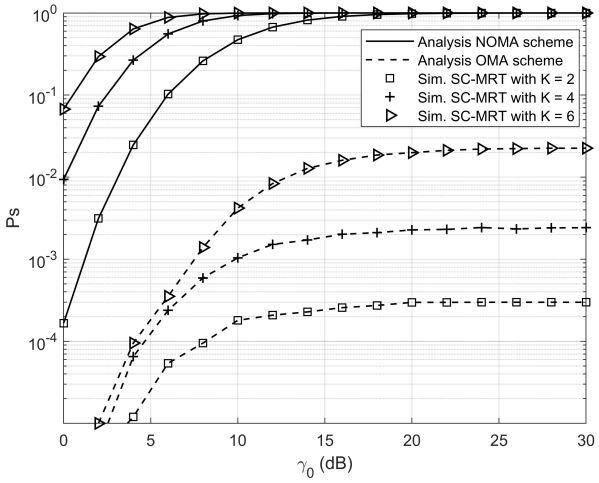

Figure 7. Impacts of the number of antennas K on Ps of SC-MRT scheme

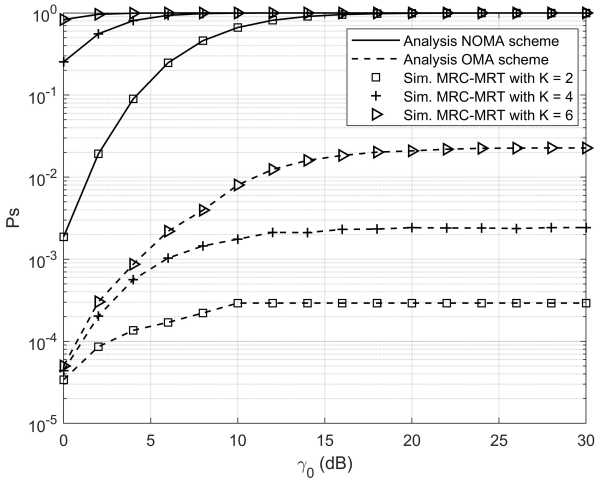

Figure 8. Impacts of the number of antennas K on Ps of MRC-MRT scheme

4.6. Optimization for successful computation probability

In Fig. 13, we verify the two optimization algorithms, i.e., **SCPMS** and **SCPMG**, to achieve the optimal performance in terms of Ps for different schemes. We can easily see that both algorithms achieve the same optimum effect for the proposed model. In order to comparison, we also plot the Ps with $\epsilon = 0.4$, $\alpha = 0.3$, and $a = 0.6$ in the non-optimal case. From this figure, we can see that when the optimization algorithm is deployed the values of Ps is higher than non-optimal ones. In other words, the computing performance of this considered system can achieve the optimal value by using the optimal set $(Ps_{\max}, \epsilon^*, \alpha^*, a^*)$ for corresponding schemes.

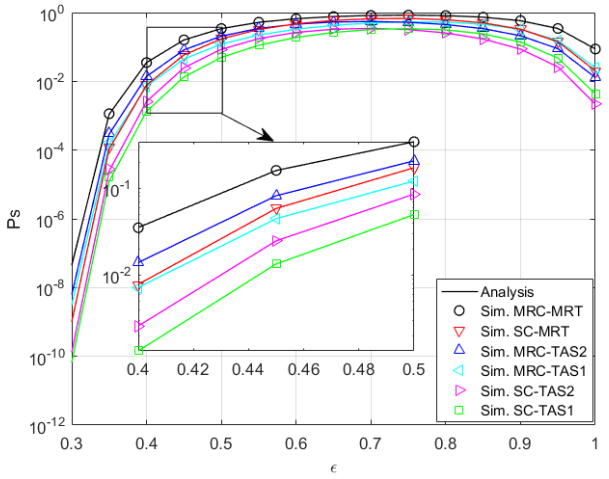

Figure 9. Impacts of the data offloading ratio ϵ on Ps of different schemes

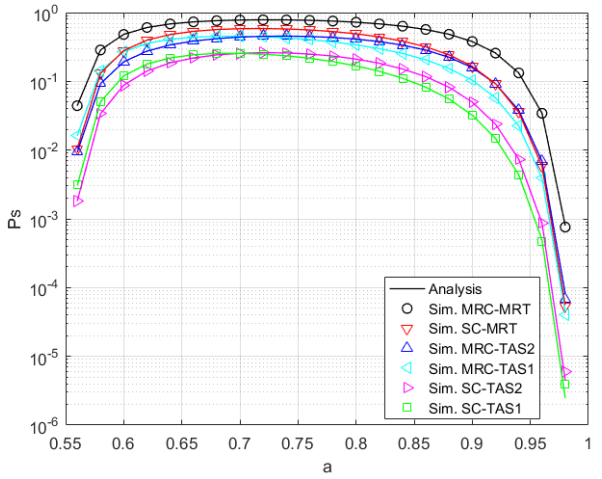

Figure 11. Impacts of the power allocation coefficient a on Ps of different schemes

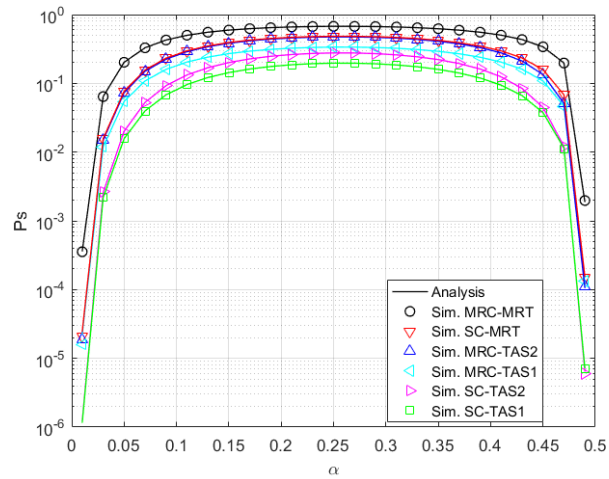

Figure 10. Impacts of the time switching ratio α on Ps of different schemes

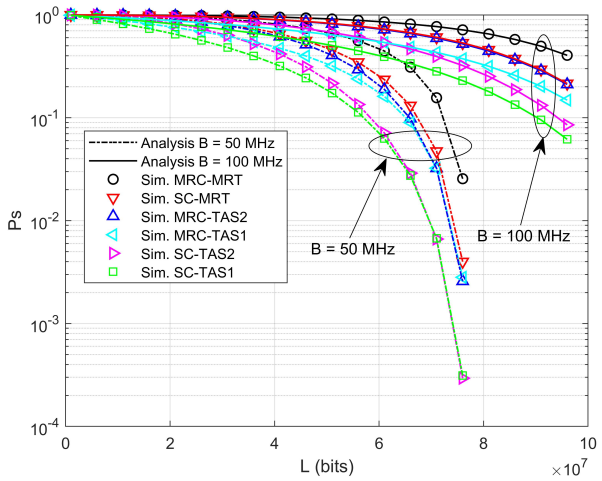

Figure 12. Impacts of the length of task and the bandwidth

5. Conclusion

In this paper, we have studied the RF energy harvesting NOMA mobile edge computing network. Six schemes, namely SC-TAS1, SC-TAS2, MRC-TAS1, MRC-TAS2, SC-MRT, and MRC-MRT are proposed for this system based on multi-antenna selection of user. We have also derived the exact closed-form expressions of successful computation probability for these corresponding schemes. Moreover, the optimization algorithm has been proposed to obtain the optimal performance. Finally, the numerical results have been provided to reveal the impacts of system parameters on performance. From these results, we observe that the performance of this considered system can be improved by increasing the transmit power and/or the number of antennas and by selecting the optimal set of key parameters: data offloading ratio, time switching ratio, and power allocation coefficient.

In our future work, we will study the case of multiple input multiple output RF EH NOMA MEC system with imperfect channel state information. We also consider the system equality and scalability to expand the scope for the study.

Appendix A. Proof of Theorem 1

Here, from equation (34) we derive the closed-form expression of Ps^{SC}_{TAS1} as (A-1) and (A-2) on the top of next page.

This ends our proof.

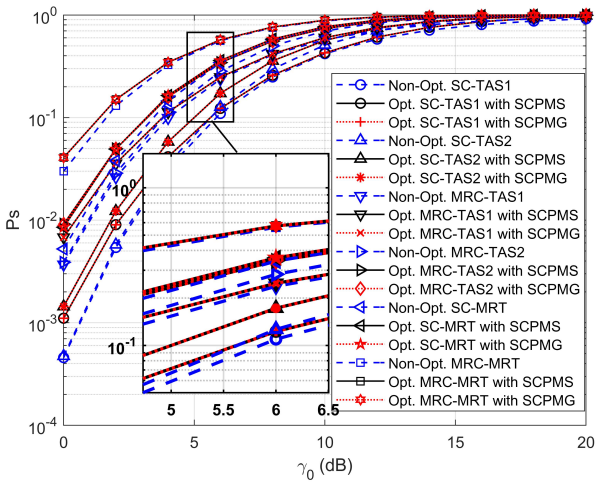

Figure 13. Optimization of Ps with different schemes

References

[1] O. Maraqa, A. S. Rajasekaran, S. Al-Ahmadi, H. Yanikomeroglu, and S. M. Sait, "A survey of rate-optimal power domain NOMA with enabling technologies of future wirelessnetworks," *IEEE*, 2020.

[2] L. Dai, B. Wang, Y. Yuan, S. Han, C. lin I, and Z. Wang, "Nonorthogonal multiple access for 5G: Solutions, challenges, opportunities, and future research trends," *IEEE Communications Magazine*, vol. 53, no. 9, pp. 74–81, 2015.

[3] A. Anwar, B.-C. Seet, M. A. Hasan, and X. J. Li, "A survey on application of non-orthogonal multipleaccess to different wireless networks," *Electronics*, vol. 8, p. 1355, 2019.

[4] Z. Ding, M. Peng, and H. V. Poor, "Cooperative non-orthogonal multiple access in 5G systems," *IEEE Communications Letters*, vol. 19, no. 8, pp. 1462–1465, 2015.

[5] A. H. Gendia, M. Elsabrouty, and A. A. Emran, "Cooperative multi-relay non-orthogonal multiple access for downlink transmission in 5g communication systems," in *2017 Wireless Days*. Porto, Portugal: IEEE, 2017.

[6] S. M. R. Islam, N. Avazov, O. A. Dobre, and K. sup Kwak, "Power-domain non-orthogonal multiple access (NOMA) in 5G systems: Potentials and challenges," *IEEE Communications Surveys & Tutorials*, vol. 19, no. 2, pp. 721–742, 2017.

[7] S. Lee, "Cooperative non-orthogonal multiple access for future wireless communications," *EAI Endorsed Transactions on Industrial Networks and Intelligent Systems*, vol. 5, no. 17, pp. 1–8, 2018.

[8] Z. Ding, Z. Yang, P. Fan, and H. V. Poor, "On the performance of non-orthogonal multiple access in 5G systems with randomly deployed users," *IEEE Signal. Process. Lett.*, vol. 21, no. 12, pp. 1501–1505, 2014.

[9] D.-D. Tran, H.-V. Tran, D.-B. Ha, and G. Kaddoum, "Cooperation in NOMA networks under limited user-to-user communications: Solution and analysis," in *IEEE Wireless Communications and Networking Conference (WCNC)*, 15-18/4/2018, Barcelona, Spain.

[10] D.-D. Tran and D.-B. Ha, "Secrecy performance analysis of QoS-based non-orthogonal multiple access networks over nakagami-m fading," in *The International Conference on Recent Advances in Signal Processing, Telecommunications and Computing (SigTelCom)*, HCMC, Vietnam, 2018.

[11] Z. Zhao and W. Chen, "An adaptive switching method for sum rate maximization in downlink MISO-NOMA systems," in *GLOBECOM 2017 - 2017 IEEE Global Communications Conference*, 2017.

[12] T. N. Do, D. B. da Costa, T. Q. Duong, and B. An, "Improving the performance of cell-edge users in MISO-NOMA systems using TAS and SWIPT-based cooperative transmissions," *IEEE Transactions on Green Communications and Networking*, vol. 2, no. 1, pp. 49–62, 2018.

[13] T. N. Kieu, D.-D. Tran, D.-B. Ha, and M. Voznak, "On secure QoS-based NOMA networks with multiple antennas and eavesdroppers over nakagami-m fading," *IETE Journal of Research*, pp. 1–13, 2019.

[14] Y. Mao, C. You, J. Zhang, K. Huang, and K. B. Letaief, "A survey on mobile edge computing: The communication perspective," *IEEE Communications Survey Tutorials*, vol. 19, no. 4, pp. 2322–2358, 2017.

[15] H. Sun, F. Zhou, and R. Q. Hu, "Joint offloading and computation energy efficiency maximization in a mobile edge computing system," *IEEE Transactions on Vehicular Technology*, vol. 68, no. 3, pp. 3052–3056, 2019.

[16] Y. Zhang, X. Lan, Y. Li, L. Cai, and J. Pan, "Efficient computation resource management in mobile edge-cloud computing," *IEEE Internet of Things Journal*, vol. 6, no. 2, pp. 3455–3466, 2019.

[17] Q. Li, J. Zhao, and Y. Gong, "Computation offloading and resource allocation for mobile edge computing with multiple access points," *IET Communications*, vol. 13, no. 17, pp. 2668–2677, 2019.

[18] W. Lu, B. Yin, G. Huang, and B. Li, "Edge caching strategy design and reward contract optimization for uAV-enabled mobile edge networks," *EURASIP Journal on Wireless Communications and Networking*, vol. 2020:38, pp. 1–10, 2020.

[19] F. Wang, J. Xu, and Z. Ding, "Optimized multiuser computation offloadingwith multi-antenna NOMA," in *2017 IEEE Globecom Workshops (GCWkshps)*, Singapore, 4-8 Dec. 2017 2017, pp. 1–7.

[20] ——, "Multi-antenna NOMA for computation offloading in multiuser mobile edge computing systems," *IEEE Transactionson Communications*, vol. 67, no. 3, pp. 2450–2463, 2018.

[21] Y. Ye, G. Lu, R. Q. Hu, and L. Shi, "On the performance and optimization for MEC networks using uplink NOMA," in *IEEE International Conference on Communications Workshops (ICC Workshops), Shanghai, China.* IEEE, 2019.

[22] Z. Ding, P. Fan, and H. V. Poor, "Impact of non-orthogonal multiple access on the offloading of mobile edge computing," *IEEE Trans. Commun.*, vol. 67, no. 1, pp. 375–390, 2019.

[23] X. Lu, P. Wang, D. Niyato, D. I. Kim, and Z. Han, "Wireless networks with RF energy harvesting: A

$$
\begin{aligned}
Ps_{TAS1}^{SC} &= \Pr\left(\max\left\{t_1+\frac{c_1\epsilon L}{f_1}, t_2+\frac{c_2(1-\epsilon)L}{f_2}\right\} < (1-\alpha)T\right) \\
&= \Pr\left(t_1+\frac{c_1\epsilon L}{f_1} < (1-\alpha)T, \quad t_2+\frac{c_2(1-\epsilon)L}{f_2} < (1-\alpha)T\right) \\
&= \Pr\left(\gamma_{AP_1}^{s_1} > 2^{\frac{\epsilon L}{(1-\alpha)B\Omega_1}}-1, \gamma_{AP_2}^{s_2} > 2^{\frac{(1-\epsilon)L}{(1-\alpha)B\Omega_2}}-1\right) \\
&= \Pr\left(\frac{ab\gamma_0 g_0 g_1}{(1-a)b\gamma_0 g_0 g_1+1} > 2^{\frac{\epsilon L}{(1-\alpha)B\Omega_1}}-1, (1-a)b\gamma_0 g_0 g_2 > 2^{\frac{(1-\epsilon)L}{(1-\alpha)B\Omega_2}}-1\right) \\
&= \begin{cases} 0, & \text{if } a<\rho \\ \underbrace{\int_0^\infty \left[1-F_{g_1}\left(\frac{\Psi_1}{x}\right)\right]\left[1-F_{g_2}\left(\frac{\Psi_2}{x}\right)\right] f_{g_0}(x)dx}_{I_{TAS1}^{SC}}, & \text{if } a>\rho \end{cases}
\end{aligned}
\tag{A-1}
$$

where $\rho = 1-\frac{1}{2^{\frac{c_1\epsilon L}{\Omega_1 B}}}$, $\Psi_1 = \frac{2^{\frac{\epsilon L}{(1-\alpha)B\Omega_1}}-1}{\gamma_s\left[a-(1-a)\left(2^{\frac{\epsilon L}{(1-\alpha)B\Omega_1}}-1\right)\right]}$, $\Psi_2 = \frac{2^{\frac{(1-\epsilon)L}{(1-\alpha)B\Omega_2}}-1}{(1-a)\gamma_s}$, $\Omega_1 = (1-\alpha)T-\frac{c_1\epsilon L}{f_1}$, $\Omega_2 = (1-\alpha)T-\frac{c_2(1-\epsilon)L}{f_2}$.

Substituting (23), (24) and (26) into the integral I_{TAS1}^{SC}, after some manipulation, we obtain

$$
\begin{aligned}
I_{TAS1}^{SC} &= \sum_{k_0=1}^{K}\sum_{k_1=1}^{K}\sum_{l=0}^{m_2-1}\sum_{\sigma_0=k_0}\sum_{\sigma_1=k_1}\frac{1}{l!}\Phi_0\Phi_1\Psi_1^{\varphi_1}\Psi_2^{\varphi_2}\left(\frac{m_2}{\lambda_2}\right)^l\int_0^\infty x^{\varphi_0-\varphi_1-l-1}e^{-\left(\frac{k_1m_1\Psi_1}{\lambda_1}+\frac{m_2\Psi_2}{\lambda_2}\right)\frac{1}{x}-\frac{k_0m_0}{\lambda_0}x}\left(\varphi_0-\frac{k_0m_0}{\lambda_0}x\right)dx \\
&\overset{(a)}{=} \sum_{k_0=1}^{K}\sum_{k_1=1}^{K}\sum_{l=0}^{m_2-1}\sum_{\sigma_0=k_0}\sum_{\sigma_1=k_1}\frac{1}{l!}\Phi_0\Phi_1\Psi_1^{\varphi_1}\Psi_2^{\varphi_2}\left(\frac{m_2}{\lambda_2}\right)^l\left[2\varphi_0\left(\frac{\beta_1}{\mu_1}\right)^{\frac{v_1}{2}}\mathcal{K}_{v_1}\left(2\sqrt{\beta_1\mu_1}\right)\right. \\
&\qquad \left. -2\mu_1\left(\frac{\beta_1}{\mu_1}\right)^{\frac{v_1+1}{2}}\mathcal{K}_{v_1+1}\left(2\sqrt{\beta_1\mu_1}\right)\right],
\end{aligned}
\tag{A-2}
$$

where $v_1=\varphi_0-\varphi_1-l$, $\beta_1=\frac{k_1m_1\Psi_1}{\lambda_1}+\frac{m_2\Psi_2}{\lambda_2}$, $\mu_1=\frac{k_0m_0}{\lambda_0}$, and $\mathcal{K}_v(.)$ is the modified Bessel function of the second kind and v^{th} order. Note that step (a) is obtained by the aid of [38, Equation (3.471.9)].

contemporary survey," *IEEE Communications Surveys and Tutorials, 17(2)*, pp. 757–789, 2014.

[24] D.-B. Ha, D.-D. Tran, V. Tran-Ha, and E.-K. Hong, "Performance of amplify-and-forward relaying with wireless power transfer over dissimilar channels," *Elektronika ir Elektrotechnika Journal*, vol. 21, no. 5, pp. 90–95, 2015.

[25] D.-B. Ha and Q. S. Nguyen, "Outage performance of energy harvesting DF relaying NOMA networks," *Mobile Networks and Applications*, 2017.

[26] X. Pei, W. Duan, M. Wen, Y.-C. Wu, H. Yu, and V. Monteiro, "Socially-aware joint resource allocation and computation offloading in noma-aided energy harvesting massive iot," *IEEE Internet of Things Journal*, 2020.

[27] C. Li, J. Tang, Y. Zhang, X. Yan, and Y. Luo, "Energy efficient computation offloading for nonorthogonal multiple access assisted mobile edge computing with energy harvesting devices," *Computer Networks*, vol. 164, p. 106890, 2019.

[28] F. Wang and X. Zhang, "Dynamic computation offloading and resource allocation over mobile edge computing networks with energy harvesting capability," in *IEEE International Conference on Communications (ICC)*, Kansas City, MO, USA, May 2018.

[29] F. Zhou, Y. Wu, R. Q. Hu, and Y. Qian, "Computation efficiency in a wireless-powered mobile edge computing network with NOMA," in *IEEE International Conference on Communications (ICC), Shanghai, China, 20-24 May 2019*, 2019.

[30] F. Giust, V. Sciancalepore, D. Sabella, M. C. Filippou, S. Mangiante, W. Featherstone, and D. Munaretto, "Multi-access edge computing: The driver behind the wheel of 5g-connected cars," *IEEE Communications Standards Magazine*, vol. 2, no. 3, pp. 66–73, 2018.

[31] P. Varga, J. Peto, A. Franko, D. Balla, D. Haja, F. Janky, G. Soos, D. Ficzere, M. Maliosz, and L. Toka, "5g support for industrial iot applications–challenges, solutions, and research gaps," *Sensors*, vol. 20, no. 3, p. 828, 2020.

[32] L. Tao, Z. Li, and L. Wu, "Outlet: outsourcing wearable computing to the ambient mobile computing edge," *IEEE Access*, vol. 6, pp. 18 408–18 419, 2018.

[33] A. Dogay and K. K. Gunes, "Diversity combining for RF energy harvesting," in *IEEE 85th Vehicular Technology Conference (VTC Spring)*, Sydney, NSW, Australia, Jun. 2017, pp. 1–5.

[34] J. Xia, L. Fan, N. Yang, Y. Deng, T. Q. Duong, G. K. Karagiannidis, and A. Nallanathan, "Opportunistic access point selection for mobile edge computing networks," *IEEE Transactions on Wireless Communications*, 2020.

[35] Y. Ye, R. Q. Hu, G. Lu, and L. Shi, "Enhance latency-constrained computation in mec networks using uplink noma," *IEEE Transactions on Communications*, vol. 68, no. 4, pp. 2409–2425, 2020.

[36] Q. Gu, G. Wang, J. Liu, R. Fan, D. Fan, and Z. Zhong, "Optimal offloading with non-orthogonal multiple access in mobile edge computing," in *2018 IEEE Global Communications Conference (GLOBECOM)*. IEEE, 2018, pp. 1–5.

[37] Y. Wu, L. P. Qian, K. Ni, C. Zhang, and X. Shen, "Delay-minimization nonorthogonal multiple access enabled multi-user mobile edge computation offloading," *IEEE Journal of Selected Topics in Signal Processing*, vol. 13, no. 3, pp. 392–407, 2019.

[38] I. Gradshteyn and I. Ryzhik, *Table of Integrals, Series, and Products*, D. Zwillinger, Ed. Elsevier Academic Press, 2007.

Dac-Binh Ha received the B.S. degree in Radio Technique, the M.Sc. and Ph.D. degree in Communication and Information System from Huazhong University of Science and Technology (HUST), China in 1997, 2006, and 2009, respectively. He is currently the Dean of Faculty of Electrical and Electronics Engineering, Duy Tan University, Da Nang, Vietnam. His research interests include secrecy physical layer communications, MIMO systems, combining techniques, cooperative communications, cognitive radio, wireless energy harvesting networks and image processing. He has published several papers on ISI/SCI/SCIE index journals, such as IEICE Transactions, Journal of Communications and Network, Wireless Communications and Mobile Computing, IETE Journal of Research, Elektronika ir Elektrotechnika, Wireless Personal Communications, IET Communications, Mobile Networks and Applications, IEEE Access, and IEEE System.

Van-Truong Truong received a B.S. degree in Electronics and Telecommunication Engineering and an M.Sc. in Electronic Engineering from the University of Da Nang, Vietnam. He is currently a Ph.D. student and lecturer of the Faculty of Electrical and Electronics Engineering, Duy Tan University, Da Nang, Vietnam. His research interests include non-orthogonal multiple access, wireless sensor networks, mobile edge computing and the IoT.

Yoonill Lee is currently a faculty of Electrical Engineering Technology at the College of Lake County, Grayslake, IL. He earned his B.S. and M.S. in Electrical Engineering from Yonsei University in Seoul, South Korea, in 1984, 1986, respectively, and M.S. in Electrical Engineering from Oklahoma State University in Stillwater, OK in 1992, and Ph.D. in Electrical Engineering from the University of South Florida in Tampa, FL in 2001. He worked at Cisco Systems as a communications engineer. His research interests include CDMA, Multi-Carrier Systems, MIMO Technology, and Physical Layer Security in Wireless Communication Systems. He has published several papers for IEEE and holds a U.S. patent.